Title

Technological developments and accelerator improvements for the FRIB beam power ramp-up

Authors

Wei, J

Alleman, C

Ao, H

et al.

SISSA

TECHNICAL REPORT • OPEN ACCESS

Technological developments and accelerator improvements for the FRIB beam power ramp-up

View the article online for updates and enhancements.

68th ICFA ADVANCED BEAM DYNAMICS WORKSHOP ON HIGH-INTENSITY AND HIGH-BRIGHTNESS HADRON BEAMS — HB2023

Technological developments and accelerator improvements for the FRIB beam power ramp-up

J. Wei [a,*] C. Alleman,[a] H. Ao,[a] B. Arend,[a] D. Barofsky,[a] S. Beher,[a] G. Bollen,[a] N. Bultman,[a] F. Casagrande,[a] W. Chang,[a] Y. Choi,[a] S. Cogan,[a] P. Cole,[a] C. Compton,[a] M. Cortesi,[a] J. Curtin,[a] K. Davidson,[a] S. Di Carlo,[a] X. Du,[a] K. Elliott,[a] B. Ewert,[a] A. Facco,[a,b] A. Fila,[a] K. Fukushima,[a] V. Ganni,[a] A. Ganshyn,[a] T. Ginter,[a] T. Glasmacher,[a] A. Gonzalez,[a] Y. Hao,[a] W. Hartung,[a] N. Hasan,[a] M. Hausmann,[a] K. Holland,[a] H. C. Hseuh,[a] M. Ikegami,[a] D. Jager,[a] S. Jones,[a] N. Joseph,[a] T. Kanemura,[a] S. H. Kim,[a] C. Knowles,[a] T. Konomi,[a] B. Kortum,[a] N. Kulkarni,[a] E. Kwan,[a] T. Lange,[a] M. Larmann,[a] T. Larter,[a] K. Laturkar,[a] M. LaVere,[a] R. E. Laxdal,[a,c] J. LeTourneau,[a] Z.-Y. Li,[a] S. Lidia,[a] G. Machicoane,[a] C. Magsig,[a] P. Manwiller,[a] F. Marti,[a] T. Maruta,[a] E. Metzgar,[a] S. Miller,[a] Y. Momozaki,[a,d] M. Mugerian,[a] D. Morris,[a] I. Nesterenko,[a] C. Nguyen,[a] P. Ostroumov,[a] M. Patil,[a] A. Plastun,[a] L. Popielarski,[a] M. Portillo,[a] A. Powers,[a] J. Priller,[a] X. Rao,[a] M. Reaume,[a] S. Rodriguez,[a] S. Rogers,[a] K. Saito,[a] B. M. Sherrill,[a] M. K. Smith,[a] J. Song,[a] M. Steiner,[a] A. Stolz,[a] O. Tarasov,[a] B. Tousignant,[a] R. Walker,[a] X. Wang,[a] J. Wenstrom,[a] G. West,[a] K. Witgen,[a] M. Wright,[a] T. Xu,[a] Y. Yamazaki,[a] T. Zhang,[a] Q. Zhao,[a] S. Zhao,[a] P. Hurh,[e] S. Prestemon[f] and T. Shen[f]

[a]*Facility for Rare Isotope Beams, Michigan State University,*
 640 South Shaw Lane, East Lansing, MI, U.S.A.

[b]*INFN — Laboratori Nazionali di Legnaro,*
 Viale dell'Università, 2 — 35020 Legnaro (Padova), Italy

[c]*TRIUMF,*
 4004 Wesbrook Mall, Vancouver, BC, Canada

[d]*Argonne National Laboratory,*
 9700 S. Cass Avenue, Lemont, IL, U.S.A.

[e]*Fermi National Accelerator Laboratory,*
 Kirk Road and Pine Street, Batavia, IL, U.S.A.

[f]*Lawrence Berkeley National Laboratory,*
 1 Cyclotron Road, Berkeley, CA, U.S.A.

E-mail: wei@frib.msu.edu

*Corresponding author.

ABSTRACT: The Facility for Rare Isotope Beams (FRIB) began operation with 1 kW beam power for scientific users in May 2022 upon completion of 8 years of project construction. The ramp-up to the ultimate beam power of 400 kW, planned over a 6-year period, will enable the facility to reach its full potential for scientific discovery in isotope science and applications. In December 2023, a record-high beam power of 10.4 kW uranium was delivered to the target. Technological developments and accelerator improvements are being made over the entire facility and are key to completion of the power ramp-up. Major technological developments entail the phased deployment of high-power beam-intercepting systems, including the charge strippers, the charge selection systems, the production target, and the beam dump, along with support systems, including non-conventional utilities (NCU) and remote handling facilities. Major accelerator improvements include renovations to aging legacy systems associated with experimental beam lines and system automation for improved operational efficiency and better machine availability. Experience must be gained to safely handle the increased radiological impacts associated with high beam power; extensive machine studies and advanced beam tuning procedures are needed to minimize uncontrolled beam losses for the desired operating conditions. This paper discusses the technological developments and accelerator improvements with emphasis on major R&D efforts.

Contents

1 Introduction

The Facility for Rare Isotope Beams (FRIB) was completed in April 2022, on scope, on cost, and ahead of the baseline schedule established about 10 years ago [1]. The ramp-up to the ultimate design beam power of 400 kW is planned over a six-year period; 1 kW was delivered for initial user runs starting in May 2022; 5 kW was delivered in February 2023. Starting in July 2023, test runs and

user runs with 10 kW beams of ^{36}Ar, ^{48}Ca, and ^{28}Si were conducted. Primary beams delivered for rare isotope production include ^{22}Ne, ^{28}Si, ^{36,40}Ar, ^{48}Ca, ^{64,70}Zn, ^{82}Se, ^{86}Kr, ^{124}Xe, and ^{198}Pt. In December 2023, a record-high beam power of 10.4 kW uranium was delivered to the target, producing rare isotopes that were separated and analyzed in the Advanced Rare Isotope Separator (ARIS).

Figure 1 compares the FRIB beam power to that of other proton and heavy ion accelerators. The goal of 400 kW for the FRIB beam power ramp-up is an order of magnitude higher than has been demonstrated so far with heavy ion accelerators.
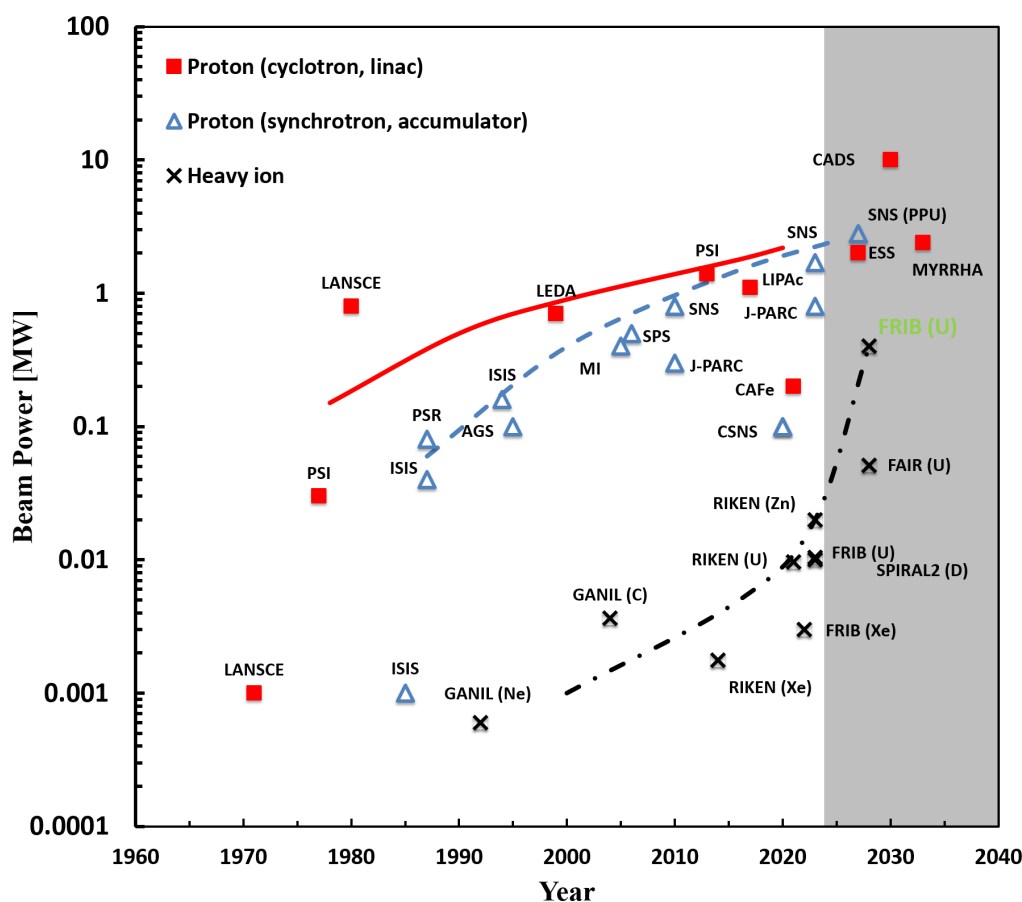
Figure 1. Beam power on target as a function of time for existing (white background) and planned (gray background) power-frontier accelerator facilities. (Data as of December 2023.)

Figure 2 shows the layout of the FRIB accelerator, beam delivery systems, and experimental areas. During the first 12 months of user operations, the FRIB accelerator complex delivered 1530 beam hours to nine science experiments conducted with primary beams at energies > 200 MeV per nucleon (MeV/u) and 2724 hours for beam developments, studies, and tuning, for a total of 4254 beam hours delivered by the full linac. Additionally, 998 beam hours were delivered to industrial users and non-scientific programs via the FRIB Single Event Effect (FSEE) beam line (with acceleration through the first linac segment only), corresponding to a grand total of 5252 beam hours. More than 200 rare isotope beams were produced by the FRIB target and delivered to user stations. The facility availability was 91.5% for scientific users and 97.2% for the industrial users.

Figure 2. FRIB layout. The underground driver linac consists of three straight segments, Linac Segment 1 through Linac Segment 3 (LS1, LS2, LS3), and two folding segments (FS1, FS2), with charge stripping in FS1. The beam delivery system (BDS) delivers beam to the Target Hall at the linac elevation. The vertical pre-separator takes isotope beams to the ground level for transport through the fragment separator to the experimental areas.

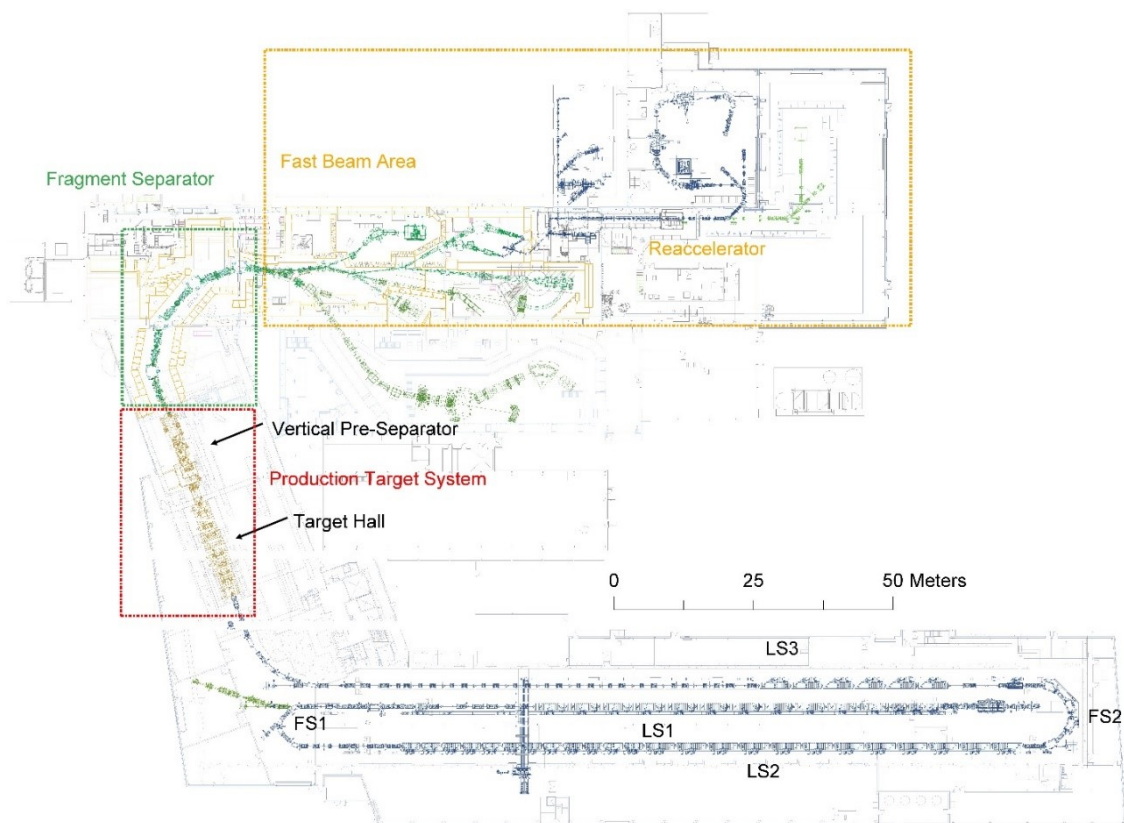Figure 3 shows the facility downtime by system category during the first year of scientific user operations. The three leading system categories were radio-frequency systems (RF), legacy cryogenics (LCR), and legacy superconducting magnets (LSM). Major contributors to RF downtime were radio-frequency quadrupole (RFQ) amplifier water leaks, low-level RF phase calibration firmware issues, and solid-state power supply failures. The LCR and LSM downtime was mainly due to aging systems newly reconfigured for FRIB operations.

Extensive development work was done to prepare for high-power operation, including work in the following areas: simultaneous acceleration of multiple charge states [2]; charge stripping of primary beams with liquid lithium [3]; development of a superconducting electron-cyclotron-resonance ion source (SC-ECR) [4]; and development of a rotating graphite target [5].

The superconducting radio-frequency (SRF) driver linac has been operating in continuous-wave (CW) mode since linac beam commissioning [6]. A total of 324 SRF cavities are housed in a total of 46 cryomodules. Each cavity is powered by a dedicated RF system, such that its amplitude and phase can be set independently. Cavity phases are optimized with a pulsed, low-average-power beam, while all experiments use a CW beam.

The SRF cavity performance during operation is shown in figure 4. The accelerating gradients are administratively-limited such that field-emission-induced X-rays do not exceed 10 to 30 mR/hr;
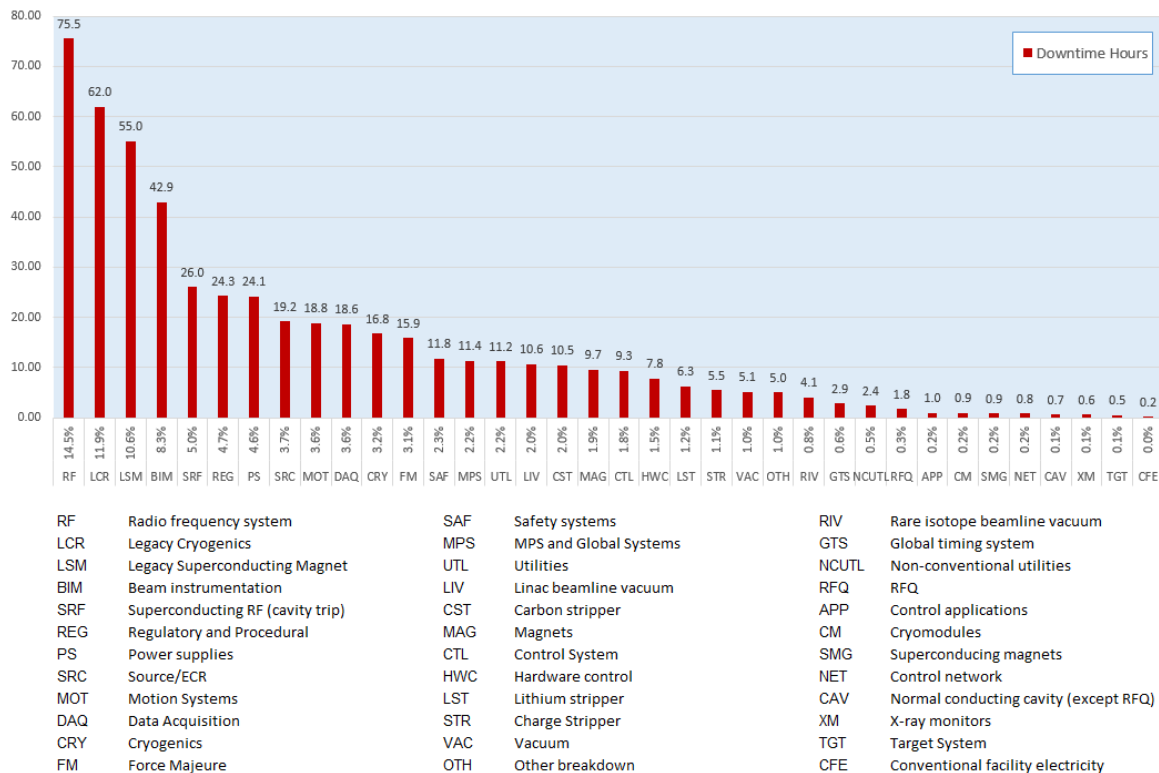
RF	Radio frequency system	SAF	Safety systems	RIV	Rare isotope beamline vacuum
LCR	Legacy Cryogenics	MPS	MPS and Global Systems	GTS	Global timing system
LSM	Legacy Superconducting Magnet	UTL	Utilities	NCUTL	Non-conventional utilities
BIM	Beam instrumentation	LIV	Linac beamline vacuum	RFQ	RFQ
SRF	Superconducting RF (cavity trip)	CST	Carbon stripper	APP	Control applications
REG	Regulatory and Procedural	MAG	Magnets	CM	Cryomodules
PS	Power supplies	CTL	Control System	SMG	Superconducing magnets
SRC	Source/ECR	HWC	Hardware control	NET	Control network
MOT	Motion Systems	LST	Lithium stripper	CAV	Normal conducting cavity (except RFQ)
DAQ	Data Acquisition	STR	Charge Stripper	XM	X-ray monitors
CRY	Cryogenics	VAC	Vacuum	TGT	Target System
FM	Force Majeure	OTH	Other breakdown	CFE	Conventional facility electricity

Figure 3. FRIB facility downtime hours by system category for full-energy beam delivery during the first year of scientific user operations. A total of 4254 beam hours were delivered, with 4649 beam hours scheduled, corresponding to 91.5% availability.

the exact limits were determined based on the performance of the cavities in offline cryomodule tests and past linac operation. For example, 5 cavities are seen in figure 4 to have maximum E_{acc} lower than the specification: this is due to field emission already observed in the cryomodule tests. For the sake of high availability and high reliability, no cavities are operated beyond the design goal. As a result, the total accelerating voltage is 98% of the design goal (as of October 2023). The beam power ramp-up will be done by increasing the average beam current without increasing the accelerating gradients of the SRF cavities.

A proactive maintenance program for the linac cryomodules is being implemented for high-reliability linac operation; for example, 3 cavities could not be used in the first year of operation, but they were recovered via warming up and in-tunnel repair in the 2023 summer maintenance period [7] and they are back in operation since October 2023. Moreover, we are developing techniques such as 'in-situ' plasma processing of FRIB SRF cavities [8] to help mitigate possible long-term degradation in cavity performance.

Although the superconducting driver linac is ready to deliver full-power beams, ramp-up of the average beam power requires facility-wide development. First, experience must be gained to safely handle increased radiological impact, including prompt radiation, activation in device materials and non-conventional utilities (NCU), and possible residual activation in ground water and exhaust air. Second, extensive machine studies and beam tuning are needed to minimize uncontrolled beam losses for the desired operating conditions. High-power targetry systems and beam-intercepting
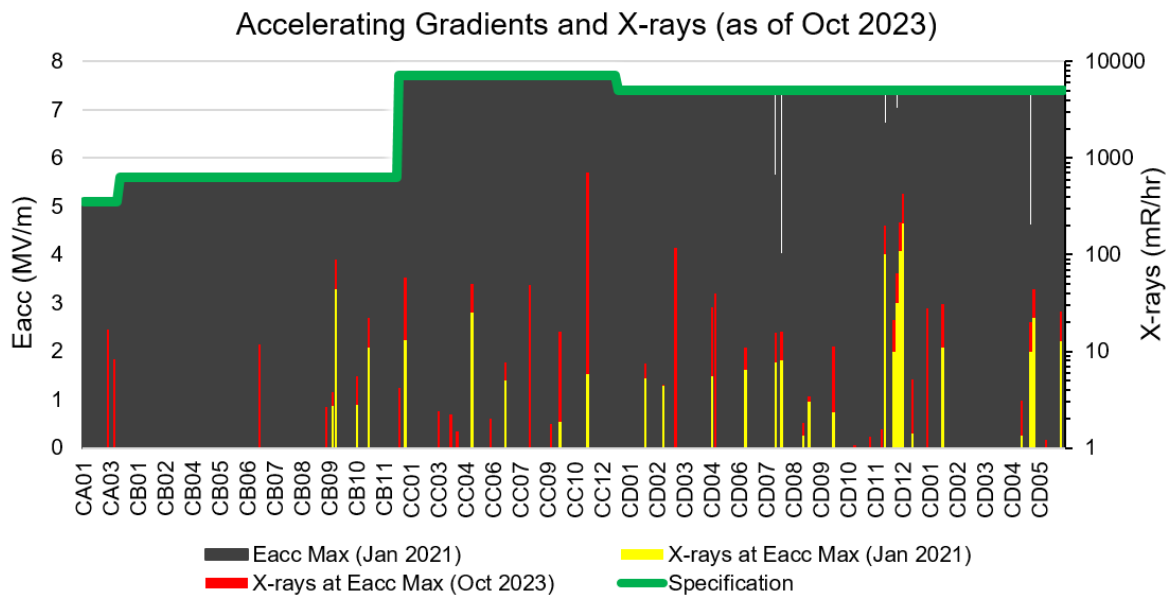
Figure 4. Performance of individual cavities in the FRIB driver linac. The maximum gradients (E_{acc}) for most cavities (black) are equal to the design goal (green). Some cavities produce field-emission X-rays (yellow, red) and are operated at reduced field. X-rays are measured by Geiger-Muller detectors, two of which are installed below each cryomodule.

devices are in phased deployment along with ancillary systems, including NCU and remote handling. Accelerator improvements and renovations to aging legacy systems are being implemented in parallel. Legacy systems inherited from the National Superconducting Cyclotron Laboratory (NSCL) reside mostly in the area downstream of the vertical pre-separator (see figure 2). During the first year of operations, the legacy cryogenic and superconducting (SC) magnet systems were among leading causes of facility downtime (figure 3).

This paper discusses the technological developments and accelerator improvements pertaining to the FRIB beam power ramp-up, with emphasis on major R&D efforts. Section 2 presents improvements to beam-intercepting devices in the driver linac including charge strippers, charge selector, and collimators; and beam intensity enhancement with ion source improvements and multi-charge-state acceleration. Phased targetry deployment is described in section 3 including the production target and beam dump, along with support systems. Section 4 discusses phased improvements in ARIS. Beam loss budget, radiological control, and personnel protection necessary to safely handle the increased radiological impacts associated with high beam power are discussed in section 5. Section 6 discusses major renovations to aging legacy systems associated with experimental beam lines inherited from NSCL. System automation for improved operational efficiency and better machine availability is discussed in section 7. Section 8 provides a perspective on the rest of the beam power ramp-up and the proposed energy upgrade.

2 Phased linac improvements

Linac improvements are planned for phased deployment to support operations and the power ramp-up, as shown in table 1. Each "epoch" corresponds to about one year. Major efforts are being

devoted to transitioning from a room-temperature ion source (ARTEMIS) to a superconducting version (SC-ECR); transitioning from the existing charge selector to higher-power versions; adding a post-stripper chicane and high-power collimators; and extending multi-charge-state acceleration to the upstream portion of the linac.

Table 1. Phased driver linac system improvements (FS: Folding Segment; BDS: Beam Delivery System).

EPOCH	1	2	3	4	5	6
Beam Power (kW)	10	20	50	100	200	400
ARTEMIS, gas beams (light ions)	🟩	🟩	🟩	🟩		
ARTEMIS, metal beams (heavy ions)	🟩	🟩				
SC-ECR, gas beams	🟩	🟩	🟩	🟩	🟩	🟩
SC-ECR, metal beams	🟩	🟩	🟩	🟩	🟩	🟩
Intermediate power charge selector in FS1			🟩	🟩		
High power charge selector in FS1					🟩	🟩
Post-stripper chicane				🟩	🟩	🟩
Additional beam collimation in FS2, BDS				🟩	🟩	🟩
Dual charge state heavy ions upstream of the stripper (velocity equalizer)					🟩	🟩

2.1 Ion source

Electron cyclotron resonance ion sources of both a normal-conducting type (ARTEMIS) and superconducting type (SC-ECR) are in operation to provide various species of primary beams needed for user experiments [4, 9]. Each ion source has a dedicated beam line, as shown in figure 5.

ARTEMIS operates at 14 GHz and is well suited to produce light and medium mass elements. It can be equipped with several ovens and sputter targets, making it quite versatile for production of beams of a wide range of elements. The room temperature magnet allows for simplified operation and maintenance.

The SC-ECR ion source contains 3 superconducting solenoids and one superconducting sextupole magnet. It is designed for operation at 28 GHz to produce high-intensity heavy ion beams. The ion source has been operated at the design magnetic field, with a maximum magnetic field of 4 T on axis and 2 T radially at the edge of the plasma chamber. It has been commissioned at 18 GHz and is fully operational for FRIB beam production at 10 kW on the production target using up to 1.5 kW
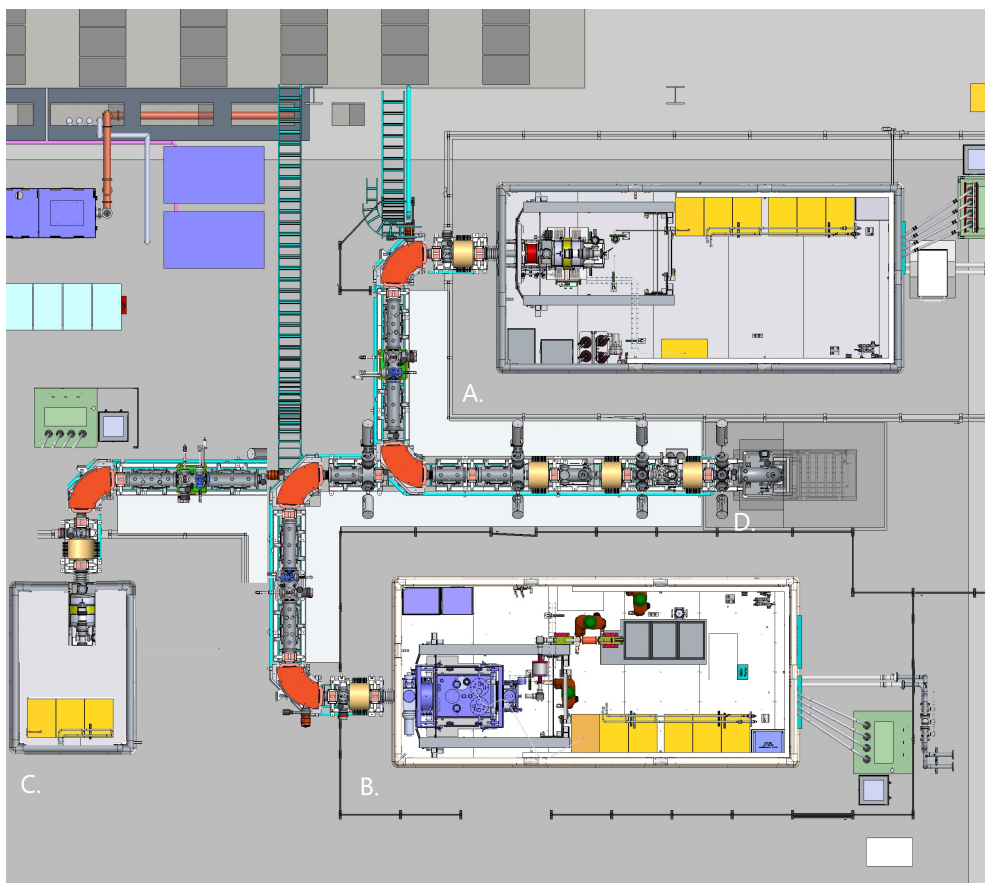
Figure 5. FRIB front end including the high-voltage platforms for two operational ECR ion sources and a third ECR ion source to be added later. A: ARTEMIS platform (14 GHz); B: SC-ECR platform (28 GHz); C: platform for a third ion source. All of the sources deliver ion beams to the LEBT where they are bent by 90° into the vertical beam line down to the linac tunnel (D).

of microwave power at 18 GHz. Integration of the ion source with a 10 kW gyrotron at 28 GHz is underway to allow the SC-ECR to support the ramp-up to 400 kW.

In the first year of FRIB operations, an oven using a cartridge heater designed for up to 600° C was used for production of lighter species (^{48}Ca, ^{70}Zn, ^{82}Se) with both ion sources. Sputtering was used for heavier species (^{198}Pt, ^{238}U). A high-temperature inductive oven has been developed to routinely reach 1800-2000 °C for higher-current Ni, Si and U beams.

A second SC-ECR source is being designed for 28 GHz operation with a Nb$_3$Sn sextupole magnet [10]; this ion source will eventually replace ARTEMIS to ensure high intensity with high availability, in particular for heavy elements such as uranium. In parallel, a third 18 GHz ion source will be added to expand the capability, versatility, availability, and reliability of the FRIB front end complex. A third beam line will be installed for the third ion source (figure 5(C)).

2.2 Velocity equalizer

The Low Energy Beam Transport (LEBT) [11] was designed to transport two-charge-state heavy-ion beams from the ion source to the linac with high reliability and high beam quality. To produce a small longitudinal emittance, the direct-current (dc) beam from the ion source is bunched upstream of
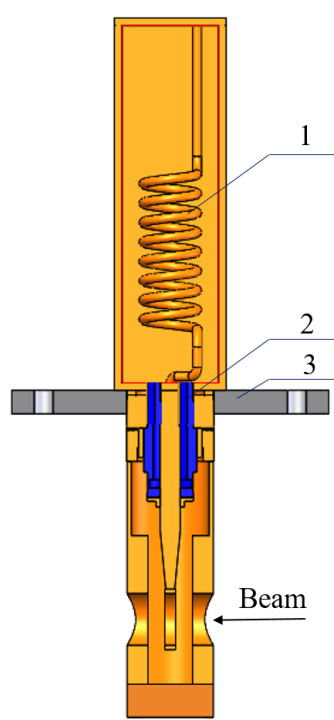
Figure 6. Sectional view of the quarter-wave resonator for the velocity equalizer. The frequency is 40.25 MHz and the required effective voltage is 1.8 kV. 1: inner conductor, 2: RF window, 3: stainless steel flange. Coiling of the inner conductor allows the resonator to be significantly more compact. Only the lower portion of the resonator is in vacuum.

the RFQ by an external multi-harmonic buncher (MHB) operating at 40.25, 80.5, and 120.75 MHz. The concept of bunching a dual-charge-state beam and injection into the RFQ is detailed in ref. [12]. When two charge states of the same ion species are accelerated with a dc voltage, the beam velocity depends on the charge state. The velocities of the different charge states must be equalized just before entering the RFQ to minimize the effective longitudinal emittance [12]. As shown in figure 6, a single-frequency 40.25 MHz resonator serves as a "velocity equalizer" (VE); it will be installed right before the RFQ. The time-of-flight (TOF) difference between the two charge states in the drift space between the MHB and VE should be equal to the RF period in the RFQ. This drift space includes a biased tube with an adjustable voltage to accommodate the required TOF of ions with masses between 200 and 238. The two-charge-state capability is not yet installed upstream of the RFQ, but will be required to produce high-power heavy ion beams above 200 kW (Epoch 5 in table 1). Overall, two-charge-state acceleration upstream of the charge stripper and acceleration of up to 5 charge states downstream of the stripper help to maximize heavy-ion power delivery to the target.

2.3 Charge strippers

The liquid lithium [3] and rotating carbon foil [7] charge strippers are installed adjacent to each other for operational flexibility. The lithium stripper is designed to work with all beams at full power. It has been successfully demonstrated with available beams, including uranium [3]. At the present power levels, there is no significant activation of materials in and around the strippers.

Valuable experience with the lithium stripper performance is being accrued during FRIB operations. Instabilities were observed in the film during extended runs; these were mitigated by replacement of the liquid filter. Efforts are being made to increase the film thickness for increased stripping efficiency, possibly by colliding two lithium jets in lieu of the current method where one jet impinges on a deflector. Trials with round water jets suggest that this approach is promising (figure 7).

Figure 7. Water film produced by colliding two jets from 1-mm diameter nozzles.

2.4 Charge selector

The charge selector is designed to intercept the charge states of the stripped heavy ion beams that do not fit into the acceptance of the downstream linac segments. The existing charge selector, a pair of copper-alloy-based water-cooled jaws, is estimated to allow for beam delivery up to 50 kW. Upgraded versions for intermediate- and high-power operations are being designed with feedback from the operational experience with the lithium stripper. In particular, accurate charge state distributions after the stripper are necessary for a reliable charge selector design, but this information was not available until the lithium stripper was commissioned.

Figure 8 shows the intermediate-power charge selector design that uses two rotating graphite cylinders to intercept the unwanted charge states, distribute the beam-induced heating over a larger area, and radiate it to the water-cooled vacuum chamber walls. The peak temperature of the graphite in the beam spot depends on many factors including the intercepted beam power, spot size, emissivity of the graphite wheels and the chamber walls, the diameter of the wheels, and the rotation speed. Our design goal is to maintain the peak temperature of the graphite wheels close to 2000 K to enhance annealing of the radiation damage and diffusion of implanted heavy ions. Full 3D heat transfer simulations show that the peak temperature can be maintained in the range from 1300 K to 2000 K (for an rms beam spot size of 0.7 mm × 1.25 mm and a beam power from 0.5 to 5 kW) by proper selection of the wheel diameter (we considered diameters of 102 mm and 152 mm). In order to mitigate cyclic thermal stress in the graphite to be below its strength limit, the wheels must rotate at > 2000 rpm.
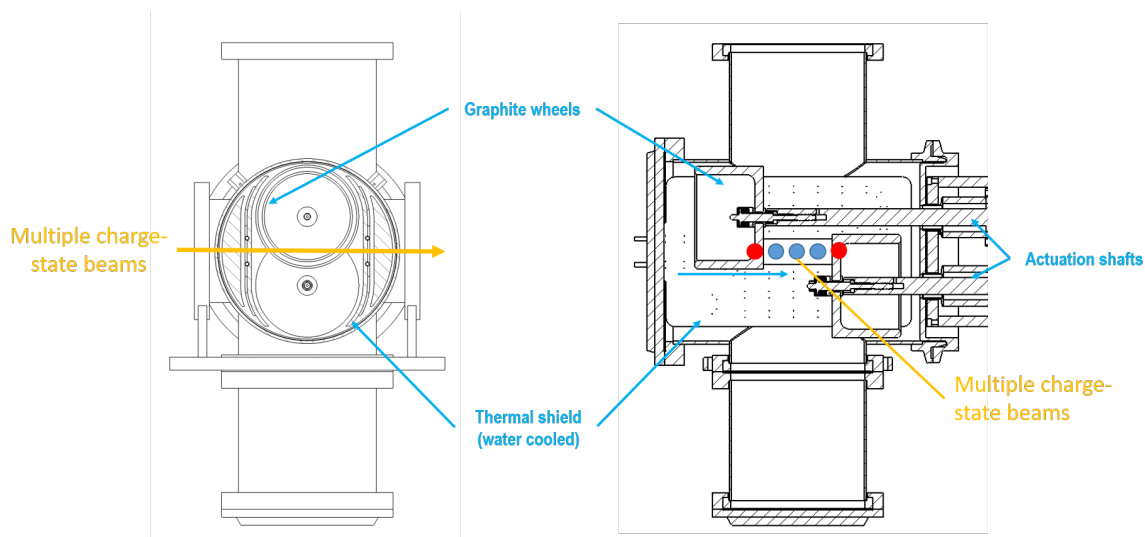
Figure 8. Sectional view of the intermediate-power charge selector conceptual design. Charge states are incident from the right with horizontal separation; the wheel positions are set to allowed transmission of 3 charge states (blue), while the rest are intercepted (red).

2.5 Collimation

The desired high beam power can be achieved with a low beam current (< 1 mA) in the CW driver linac. Hence space charge effects are mostly negligible, except in the ion source and LEBT. However, collimation is nevertheless required for several reasons:

- Filamentation of the phase space distribution occurs due to the inherent nonlinear fields in the ion source and the high space charge due to the extraction of multi-component ion beams. Efficient beam halo collimation in the LEBT is provided using two round collimators located where the LEBT beam is axially symmetric. The phase advance between the collimators is about $60°$ for efficient beam halo cleaning in the beam's phase space. We are considering installing an additional variable-aperture collimator upstream of the RFQ for further beam halo reduction.

- Contaminants (unwanted ion species produced by the source with rigidity close to that of the primary ion species) must be blocked by collimators and vacuum chambers in the post-stripper chicane and FS1. Charge stripping increases the emittance due to scattering and energy straggling. Collimation downstream of the stripper is needed to intercept particles scattered to large angles. Seven collimators were installed to intercept contaminants, ions created due to charge-exchange reactions, and beam halo produced by emittance growth [13].

- A four-segment water-cooled collimator with temperature sensors was installed upstream of the target. This collimator prevents halo particles from reaching the mirror of the beam imaging system on the target. In addition, it helps to control the beam position.

Collimation significantly reduces uncontrolled beam losses. The collimators must be properly shielded to avoid high residual radiation levels in the linac tunnel.

2.6 Beam diagnostics

Diagnostics for development and monitoring of beams in the front end, linac, and target segments have been developed and deployed [14–16]. These systems, including beam position monitors and beam current monitors, are designed to operate with beam currents from a few nA to 1 mA with adequate dynamic range for beam tuning and monitoring for the anticipated beam powers and energies.

Beam profile monitoring is typically performed with multi-wire "harp" systems that intercept beams low average power (up to 20 W); this requires severe attenuation of the beam power for multi-kilowatt beams. The maximum dynamic range in intensity with such an approach is about a factor of 10^3. Alternative methods are being developed to extend the dynamic range of profile measurements for accurate resolution of beam halo at the 10^{-5} to 10^{-6} level. Challenges include the risk of intercepting high power densities, the possibility of generating of secondary particles, and the need for safeguards to prevent contamination that may adversely impact the SRF cavities. Gas-sheet-based profile monitoring [17] is currently in development for evaluation for FRIB applications. Other techniques, including flying wires or rotating wires, are also being considered for high power profilometry. Coupling such minimally-intercepting devices with external secondary radiation monitors (see, for example, ref. [18]) may extend the practical dynamic range of intercepting devices to allow for useful transverse beam halo measurements.

3 Phased targetry deployment

Proton facilities generally have been able to delivery higher beam power than heavy-ion facilities (figure 1). One reason for this is that heavy-ion facilities face more challenges due to higher power deposition density and higher radiation damage. These are major considerations for the design of FRIB targetry and ancillary systems; these systems are in phased deployment (table 2). Although most challenges were understood at the time of the project baseline, additional complexities became clear during facility commissioning and early operation. Figure 9 shows the layout of the target, beam dump, wedge, and Advanced Rare Isotope Separator (ARIS). As seen in table 2, major items include increasing the power-handling capability of the target itself, adding a shield downstream of the target, iterative improvements to the beam dump, a redesign of the wedge system, and safety system upgrades.

The targetry lacks the fast beam-diagnostic sensors used for the linac. To mitigate this drawback, upstream magnet power supplies are monitored by interlocking machine protection systems. Further beam diagnostics are provided with thermal sensors, imaging cameras, and intercepting plates. The collimator located 1.5 m upstream of the target is segmented for position-resolved temperature monitoring. This collimator intercepts the beam halo and produces signals which are used to help align the beam onto the target.

3.1 Target

The target is expected to absorb $\sim 25\%$ of the primary beam power. Single-slice rotating graphite targets [5] are planned for a primary beam power of up to 50 kW. Multi-slice targets with an improved heat exchanger will be used for full-power beam operations.

The single-slice target consists of a graphite disc, a copper heat exchanger, a ceramic hub, and an invar spindle with bearings (figure 10). Recently, a high-emissivity coating was applied to the
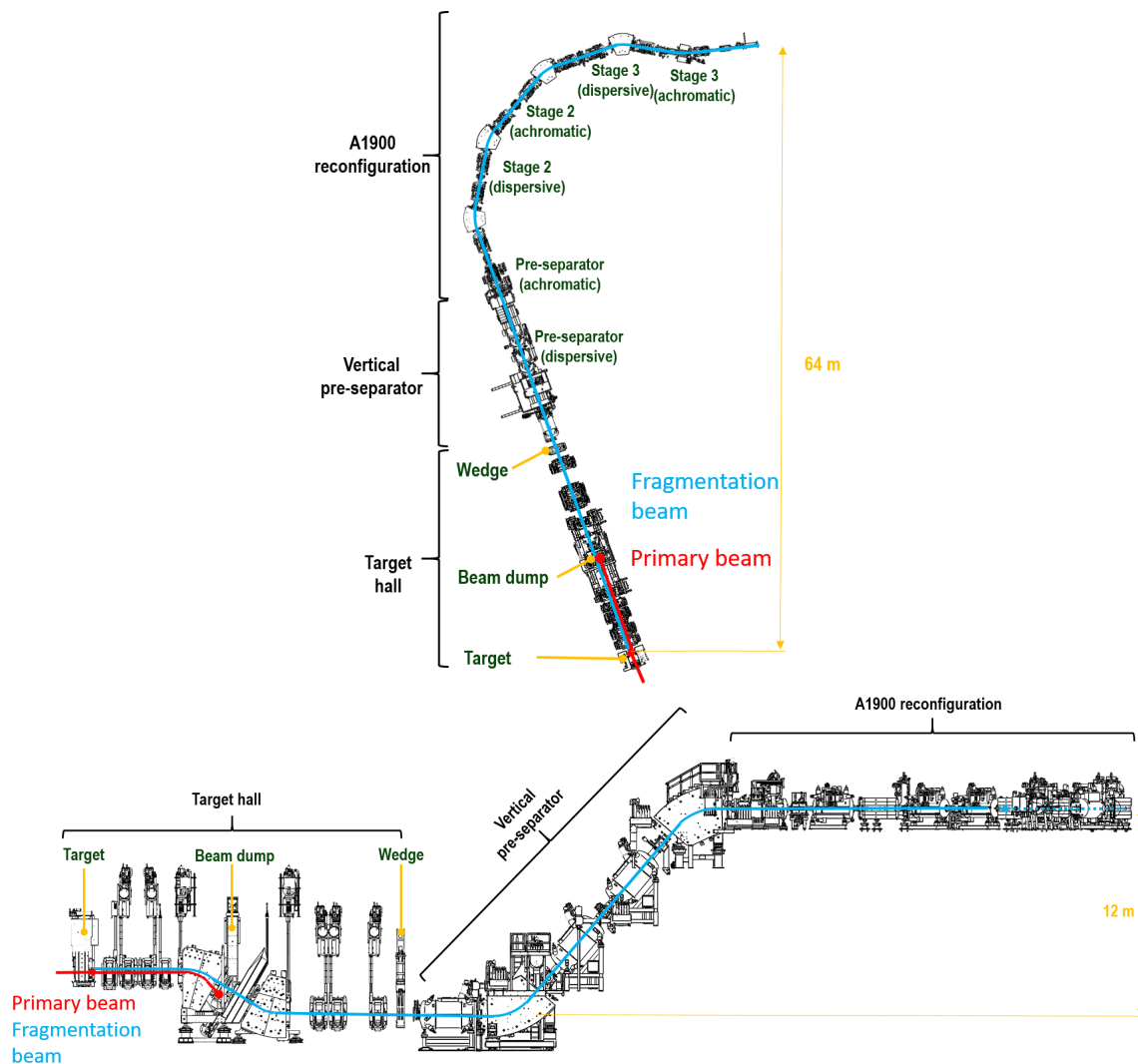
Figure 9. Layout of the Target Hall and fragment separator (ARIS). Top: top view. Bottom: elevation view. Rare isotopes are produced when the primary beam strikes the target. The beam is the directed downward to intercept the primary beam in the beam dump. Selection of the desired isotope from the fragmentation beam is done using the wedge and ARIS.

heat exchanger interior to enhance radiative cooling efficiency for the disc. High-service-temperature bearings and lubricants will be implemented for the power ramp-up.

3.2 Beam dump

The beam dump is designed to absorb ~ 75% of the primary beam power. Presently, a static aluminum water-cooled dump is used with the beam incident at a 6° angle to reduce the deposited power density. A new beam dump with an improved design (figure 11) will be installed in summer 2024. The redesigned dump will include a copper alloy layer to intercept the beam. The higher thermal conductivity of the Cu alloy will help to reduce the temperature increase due to beam heating. However, precautions are needed to ensure that the beam dump cooling water does not come into contact with the Cu alloy, as Cu is vulner-

Table 2. Phased targetry and ancillary system deployment.

EPOCH	1	2	3	4	5	6
Beam Power (kW)	**10**	**20**	**50**	**100**	**200**	**400**
Rotatable target, 1 slice	■	■	■			
Rotatable target, multi-slice			■	■	■	■
Post-target shield				■	■	■
Beam dump 6° slant (S-shape)	■	■				
Beam dump 6° slant, better cooling		■				
Rotatable beam dump, 1-mm wall			■	■	■	
Rotatable beam dump, 0.5-mm wall						■
Medium power ladder wedge system with adjustable slits (hands-on)	■	■	■			
High power wedge system (remote handling)				■	■	■
PPS upgrade with fast ionization chambers	■	■	■	■	■	■
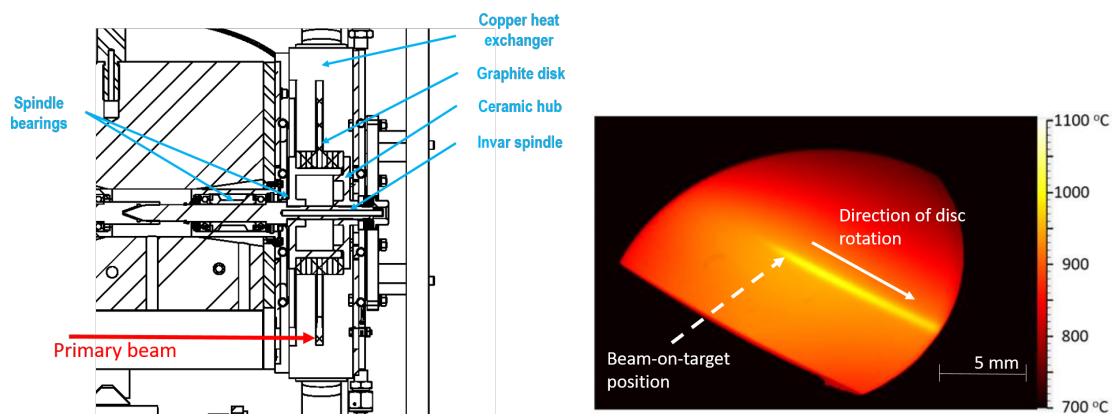
Figure 10. Left: single-slice graphite target inside the water-cooled copper enclosure. Right: thermal image of a 10.4 kW, 177 MeV/u ^{238}U beam on the graphite disc rotating at 500 revolutions per minute. The beam spot of about 1 mm diameter is near the center of the image. The yellow "tail" is due to the rotation.

able to oxidation that is enhanced by chemical reactions with oxygen produced by secondary particles interacting with the water (oxidation may result in pitting of the material). Hence the cooling channels will be made from aluminum bonded to the Cu alloy. Mini-channels will be used for more effective heat transfer to the cooling water. The ultimate beam dump (figure 12) will be a rotating thin-wall water-filled drum, with the water flow serving both to cool the wall and stop the primary beam within the drum [19].
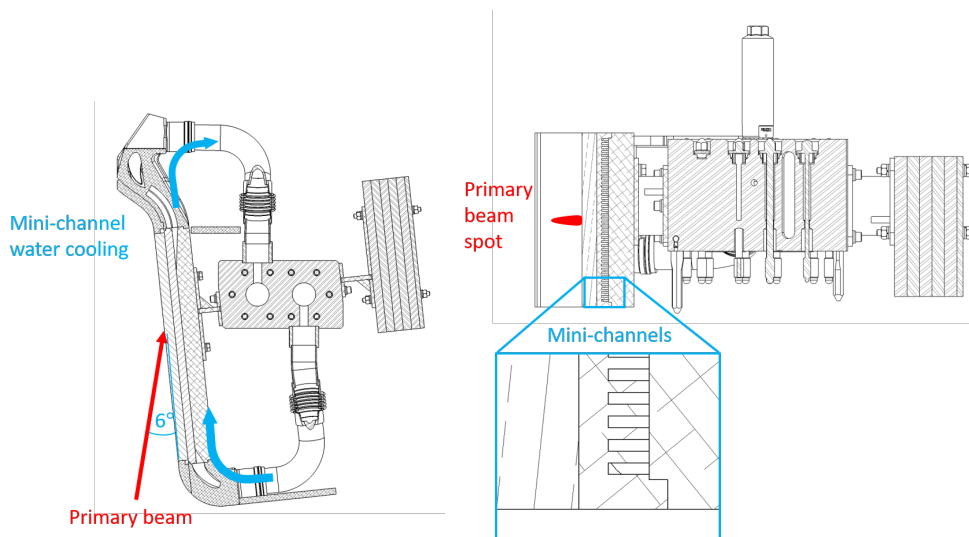
Figure 11. Intermediate mini-channel beam dump top (left) and front (right) sectional views. Inset: detail of the channels.
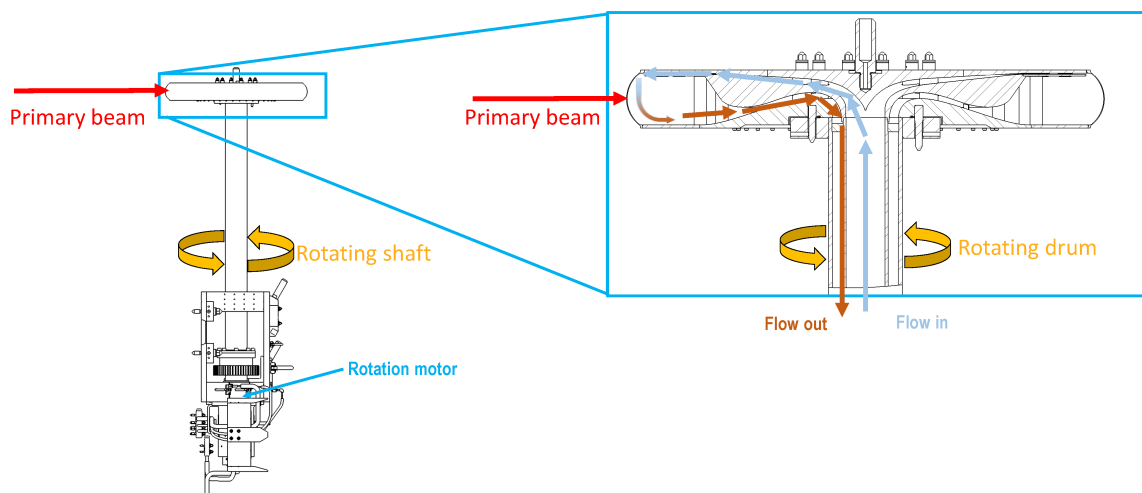
Figure 12. Rotating beam dump schematic (left) and sectional view (right).

3.3 Wedge

Secondary rare-isotope beams travel through a wedge-shaped absorber. The wedge's energy absorption is dependent on the transverse position of the ions, which allows for improved isotope separation. The wedge has a unique shape to help maintain achromaticity at the downstream focal plan where

undesired species are stopped at the slits. Wedge upgrades are planned, including the addition of remote handling capability and better tolerance to beam heating. A variable wedge system is being developed to increase tuning flexibility and operational availability.

3.4 Remote handling

With up to 400 kW of beam on target, activation and radioactive waste generation make remote handling mandatory. Our remote handling design features combine hands-on and fully-remote operations to maximize efficiency and minimize operational costs. Presently, 4 hours after turn-off, the Target Hall can be accessed by trained personnel for hands-on work to prepare for subsequent fully-remote operations to handle highly-activated components.

Remote handling is done routinely for target disc and wedge changes during user operations and annual maintenance of the beam dump within the Target Hall. An automated 4-axis 20-ton overhead crane is used to remove these devices from the beam line and move them to one of three window-equipped stations with manually-controlled through-the-wall manipulators; these stations are designed for maintenance and repair of the target and wedge systems. Tooling and procedures are newly developed for changing the target bearing cartridge and applying the high-emissivity coating to the target heat exchanger (figure 13). Duplicate target and wedge assembly modules are being developed to allow for quick reconfiguration (< 24 hours) during user experiments. These duplicate assemblies will allow reconfiguration of one assembly while the other assembly is being used. We anticipate replacing target modules regularly (every 2 weeks or so) once the duplicates are ready; wedge assembly module replacement will likely be done at a similar rate.

Flexibility in remote handling systems is an asset, as unexpected situations may arise and new procedures may be needed as the facility evolves. Although the overhead crane is automated, it can be easily reprogrammed and can store programs for many procedures; manual crane operation is possible as well when needed. As the manipulators for the 3 window stations are all manually controlled, they have built-in flexibility for new tasks and procedures.
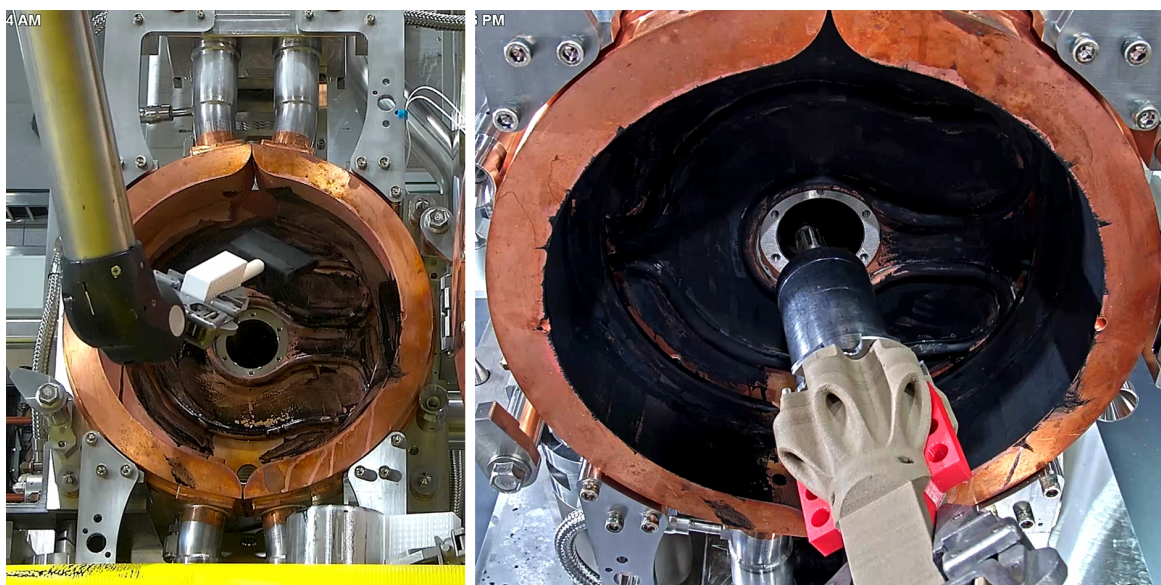

Figure 13. Target remote work: heat exchanger coating (left); bearing cartridge replacement (right).

4 Phased ARIS improvements

ARIS is used to collect and separate rare isotope beams produced at the target. ARIS includes a number of advanced design features that allow for efficient collection of fragments, with three stages of separation [20]. The separator has been commissioned and beams for more than 20 experiments have been successfully produced and delivered. With operational experience, a number of improvements are being implemented [21], as will be outlined in this section.

4.1 Diagnostic instrumentation and detectors

The pre-separator and the ARIS are equipped with multiple types of beam diagnostic instrumentation and detectors. These instruments and detectors are used to characterize the beam properties and transmission efficiency; to tune and optimize the beam prior to experiments; to ensure long-term stability and machine protection; and to provide event-by-event tracking and timing information for physics analysis.

Measurements of the beam profile for beam tuning are done with a dense set of monitors based on phosphor (Y_2O_2S:Eu) screens imaged by high-sensitivity cameras. Particle identification is done via a ToF $B\rho$-ΔE method, which allows the atomic number (Z) and mass-to-charge ratio (A/Q) of an isotope to be computed on an event-by-event basis [21]. An example of detectors used for this purpose is shown in figure 14. The magnetic rigidity ($B\rho$) is extracted from the particle positions and angles measured (tracked) using Parallel Plate Avalanche Counters (PPACs). Thin plastic scintillators coupled to a Photo-Multiplier Tube (PMT) are used for the ToF measurements, from which the atomic mass (A) is determined. The plastic scintillator assembly provides additional functions: local triggering and rate measurement. The measurement of energy loss (ΔE) to infer the atomic number (Z) is done using thin silicon PIN diodes as transmission detectors. For charge-state (Q) separation, the Total Kinetic Energy (TKE) is measured by stopping the beam particles either in a stack of Si-PIN detectors (up to several mm), or in a thick plastic scintillator material coupled to two PMTs.
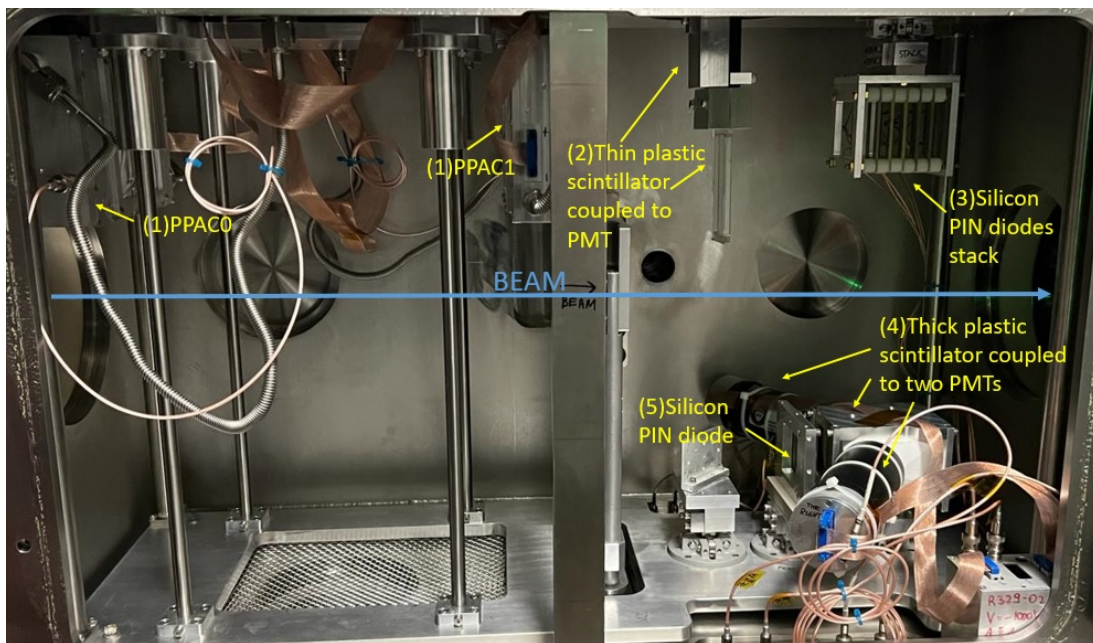

Figure 14. Diagnostics and PID detector assembly installed in the ARIS DB5 focal-plane box.

Because of the demanding FRIB performance requirements, some of the diagnostics and tracking functionality for the fragment separator had to be upgraded relative to the technologies used in the NSCL era. This includes an upgrade of the PPAC readouts from the slow charge-division based technology [22] to the fast delay-line method (DLPPAC). Using DLPPACs, the rate capability of the tracking system for the ARIS was improved by two orders of magnitude. Additionally, DLPPAC fast timing signals may be used with plastic scintillators in order to improve the accuracy of ToF measurements. Time resolution of a few hundred picoseconds can be achieved by processing the signals from the DLPPAC anode; this is comparable to that of small-area plastic scintillator detectors.

Since plastic scintillators cannot survive in a high-dose-rate radiation environment, timing measurements based on DLPPACs alone may be needed for high beam rates (approaching 1 MHz). However, some radiation-induced aging issues have been observed in DLPPACs, manifested as degradation of the electrode foil conductivity and uniformity. This aging is caused by the bombardment from an intense flux of cations produced during the gas avalanche processes, which causes the metal surface of the electrode to evaporate, leading to a gradual decrease in the detection efficiency of the device. Demetalization and rupture of the fragile electrode foils can also occur during sporadic violent discharges and from hot gas streamers. As a means of mitigating these disruptive effects and improving detector reliability and durability, alternative materials for metallic coating of the thin insulating substrates are currently under investigation (existing technology generally relies on gold or aluminum coatings of polyethylene substrates). Materials with high melting points and high electrical resistances may offer better endurance to spark effects; materials under consideration include chromium, silver, and carbon, or sandwiched layers of these materials.

An innovative approach to read out PPAC detector signals for localization is based on the large amount of scintillation light generated in a high-scintillation-yield gas, instead of the conventional charge read-out method [23]. The detector is based on a single volume filled with high-scintillating gas surrounded by collimated photodetectors (SiPMs, APDs, etc.). In this configuration, the position of the impinging beam particle is computed as the "center of gravity" of the light recorded by the array of photo-sensors. This approach was recently investigated for FRIB applications [24]. A position resolution of about 1 mm was demonstrated with a rate over a few hundred kHz with a prototype optical PPAC.

The outstanding properties of diamond as a detector medium allow the development of particle detectors with very fast time response and excellent radiation hardness. Detectors based on chemical vapor deposition (CVD) of diamond were developed at NSCL in the past. The current development projects are focused on the investigation of optical-grade detectors for large-area applications. Sub-nanosecond signal rise times provided by diamond detectors lead to excellent time resolution at a rate approaching 10^7 pps. However, due to their limited size, diamond devices can be used for ToF or energy-loss measurement only in locations where the beam size is small, e.g., near focal points along the ARIS beam line.

4.2 Magnetic corrections

Imperfect magnet alignment and imperfect beam trajectories result in horizontal and vertical offsets at the ARIS focal planes. With beam offsets, the ARIS sextupole magnets produce small dipole kicks that result in beam steering on the level of 0.01 T·m field integral or around 0.1% of the full field integral. This steering is sufficient to produce an error in the selected fragment and must therefore be corrected.

Three room temperature corrector dipoles were added to the vertical pre-separator for this purpose. The magnets have a large bore (400 mm) and magnetic field integrals of 0.016 T·m. This is sufficient to correct position offsets of approximately 5 mm and to compensate for sextupole-induced effects up to the full rigidity of ARIS (8.0 T·m). The magnets have been installed and function as expected. Additional cooling will be added to reach the full field needed for induced dipole corrections.

4.3 LISE++

The LISE++ software [25] is used to simulate fragment separators; it plays a crucial role in predicting the intensities and purities of rare isotope beams at FRIB. LISE++ is instrumental in both the planning and execution of experiments employing ARIS. LISE++ was developed at NSCL and is widely used by rare isotope beam facilities. Recently, the software was significantly updated, transitioning to the Qt framework to support modern compilers and computing methods [26]. Version 17 was released in November 2023 with substantial improvements aligned with initial ARIS operations and initial FRIB experimental results. These advancements are particularly relevant to the unique features of ARIS, including its versatile ion optics primarily designed to operate in momentum-compression mode [20].

5 Beam loss budget, radiological control, personnel protection

Managing controlled beam loss and minimizing uncontrolled beam loss are crucial for maintaining radiologically sound operations with hands-on maintenance. The "loss budget" (tables 3, 4, 5, 6) is the basis for shielding design, radiological impact control, personnel protection systems (PPS), environmental impact assessment and protection, and remote handling.

Table 3. Estimated controlled primary beam loss for typical 400 kW operation. MEBT: Medium Energy Beam Transport; F-Cup: Faraday Cup; LS: Linac Segment; FS: folding segment; RI: Rare Isotope.

Mechanism	Location	Power [kW]
Front end beam tuning	MEBT F-Cup	0.1
$\beta = 0.041$ beam tuning	LS1 Nb plate	0.002
LS1 beam tuning	FS1a dump	0.015
LS1 beam tuning	FS1b dump	0.5
Charge stripping loss	FS1 stripper	1.3
Unwanted beam collection	FS1 selector	7–12
Unwanted charge state and ion contaminants collection	FS1 45° dipoles	0.1–0.4
Beam halo and ECR ion contaminants interception	Collimator 1–5	0.1–1.7
Charge exchange halo	Collimator 6–7	0.02
LS1 beam tuning	FS1 F-Cup	0.03
LS2 beam tuning	FS2 dump	0.14
LS2 beam tuning	FS2 F-Cup	0.03
Linac beam tuning	BDS dump	0.14
Targetry protection	Collimators	0.1
RI production	Target	< 80
Spent beam	Beam dump	< 320

Table 4. Estimated controlled secondary beam loss for typical 400 kW operation.

Mechanism	Location	Power [kW]
Target scattering	Post-target shield	< 15
RI beam cleaning	Fragment catchers	< 20
Post-target scattering	Thermal armors	< 17
Post-target scattering	Collimators	< 9
RI beam	Wedge	< 2
RI beam cleaning	Wedge slits	< 3
RI beam cleaning	Separator slits	< 5
RI beam cleaning	Focal plane slits	< 2

Table 5. Estimated uncontrolled beam losses for typical 400 kW operation.

Mechanism	Location	Power
Stripper scattering	Downstream of stripper	< 3 W/m at 17 MeV/u
Uncontrolled loss	All locations	< 1 W/m

Table 6. Accidental beam loss scenarios for typical 400 kW operation. MPS: Machine Protection System; PPS: Personnel Protection System.

Mechanism	Power	Response Time	
		MPS	PPS
Damaged stripper	Small fraction of 50 kW	35 µs	N/A
Damaged target	Large fraction of 400 kW	200 µs	7 ms

5.1 Personnel protection

As FRIB is located in the middle of a university campus, the PPS must be able to shut off beam fast enough to keep the integrated dose rate below the regulatory limit in the worst-case incident scenarios. Presently, we use commercial fast neutron monitors with a total system response time < 0.3 s, which allows for intermediate-power operation with the present shielding. As we increase the beam power, another PPS layer is being added for prompt radiation hazard mitigation: the "fast beam containment system" (FBCS) consisting of ion chambers, beam inhibit devices to shut off the RFQ, and connecting optical fiber. Among various failure modes (table 6), the most demanding scenario corresponds to the primary beam being inadvertently delivered to the secondary beam line (damaged target scenario).

5.2 Non-conventional utilities

The NCU provide cooling for the targetry devices and handle transferred radioactivity accordingly. They include two closed cooling loops, centrifugal pumps, heat exchangers, gas-liquid separators, drain

tanks, and instrumentation; auxiliary systems include a hydrogen recombiner, a clean-up system, and a low-level liquid waste system. The hydrogen recombiner was recently commissioned (figure 15); it is designed to catalytically recombine H_2 produced by water radiolysis with O_2 and capture gaseous radionuclides generated during operation. The clean-up system to remove particulate and ionic impurities from the cooling water is being upgraded for remote handling capability and easier maintenance.
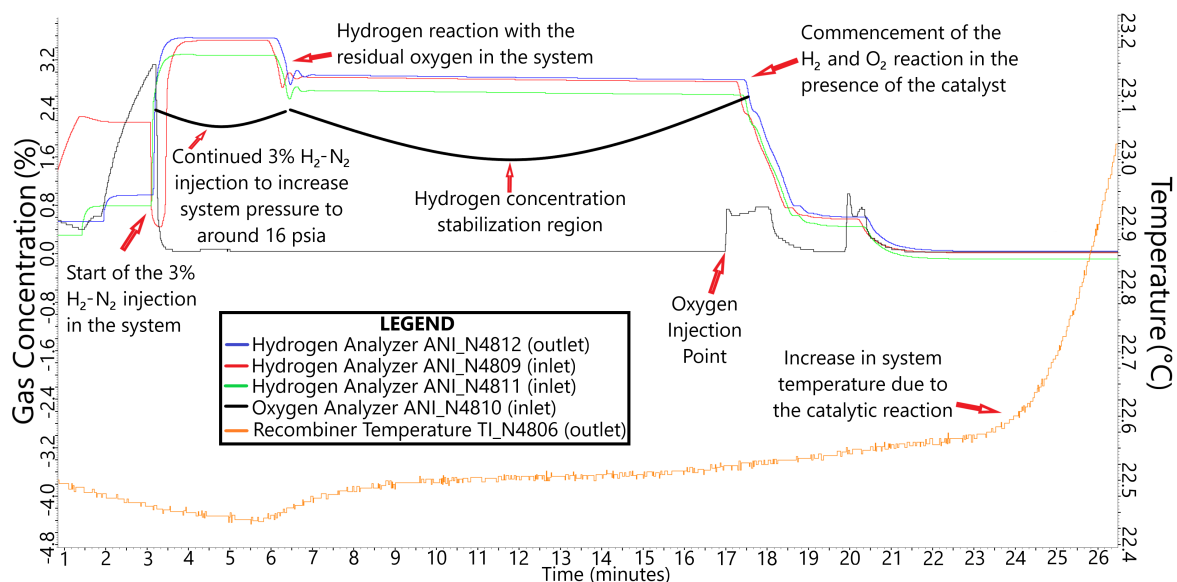

Figure 15. Concentration of H_2 and O_2 and temperature variation in the hydrogen recombiner during injection of 3% H_2-N_2 gas mixture with subsequent injection of pure O_2.

6 Legacy system renovation

6.1 Cryogenics

The FRIB central helium refrigeration system commissioned in 2018 presently supports operation of the cryomodules in the driver linac and SC magnets in the linac, Target Hall, and pre-separator area [27]. The remaining experimental areas are supported by the legacy NSCL cryogenic He refrigeration system originally designed in the mid-1970's, refurbished in 2000, and reconfigured for FRIB [28]. As seen in figure 3, the legacy cryogenics system was responsible for approximately 20% of the total downtime during the first year of scientific operations. The overall downtime in this category is due to aging equipment compounded by legacy cryostats (SC magnets) with a plethora of operational issues ranging from leaks (both insulating vacuum and cryogenic circuits) to very low design pressures, making them susceptible to frequent venting and long recovery time following a transient (quench etc.). Although segregation of the loads between the two cryogenic systems protects the FRIB central system from frequent configuration changes and contamination risks, the legacy NSCL systems must be upgraded for stability, reliability, efficiency, and support of future expansion. In addition to upgrades of the aging equipment and legacy SC magnets (discussed in section 6.2), adoption of a quench recovery system for future expansion of the facility is also being considered. The newly commissioned SC magnets for the FRIB target and pre-separator segment (designed for higher operating pressure) incorporates such a system [29, 30], which has shown excellent performance so far [31].

The cryogenic infrastructure prioritizes:

- Efficient operation to minimize the cost of utilities (electricity and liquid nitrogen), with the patented floating pressure process cycle [32], adjusting the cryoplant cycle to the loads;

- Maximum availability with adequate redundancies;

- Phased commissioning for evolving configurations, matching user needs with minimal downtime;

- Multiple independent sub-systems for maintainability, with expandability;

- Automated operation with a minimal work force.

The upgrade includes the addition of a 4.5 K cold box, a shield cold box, and a shield cold box compressor.

Recovery, purification, and preservation of the helium inventory is of critical importance. The total liquid He inventory at FRIB is ∼ 40000 liters. A high-capacity helium recovery system (including a compressor and He purifier, with at least 3 to 5 times the contaminant collection capacity compared to equivalent commercial units) is being developed for improved He preservation. Models of the helium recovery compressor and purifier are shown in figure 16, along with a photo of the purifier cold box skid. A high-pressure (200 bar) He storage system is also planned to manage the He inventory during operational transients. When completed, these systems will allow for recovery of the entire FRIB He inventory during major maintenance periods and accelerator upgrades (which may require extended down periods). The storage system will be able to accommodate a year's time worth of He inventory onsite and will provide long-term storage, minimizing the operational impact of fluctuations in the He supply chain.

6.2 Magnets

Legacy NSCL SC magnets make up ∼ 50% of the SC magnets at FRIB; they are mainly in beam lines to experimental stations. The magnets have been in service for > 20 years and present known challenges, including (i) insulating vacuum issues; (ii) flawed design features that are susceptible to introducing He leaks; and (iii) limitations in performance due to outdated magnet technology. We are currently refurbishing spare magnets to mitigate these issues. This includes replacing the vapor-cooled current lead piping and adjusting the pressure relief configurations. The refurbishment program is phased to minimize risks [33]. Simultaneously, we are developing new magnet technology using high temperature superconductors (HTS), innovative iron-free coil designs, and advanced conduction cooling. The ultimate objective is to replace all of the legacy magnets with new designs to significantly enhance operational performance.

An example of improved SC magnet development for FRIB is the Coil-Dominated Quadrupole (CDQ) under development for ARIS. The CDQ effort has progressed from the R&D phase to the manufacturing phase. The prototype coil design specifications closely resemble those of the current ARIS third-stage fragment separator triplet magnets [34]. The quadrupole coils feature a warm temperature bore of 200 mm, a maximum gradient of 18.2 T/m, and an effective length of 0.79 m. To accommodate the large aperture to effective length ratio, a Walstrom-style coil geometry [35] was chosen. This design choice aims to reduce the total cold mass weight and helium inventory by approximately four times compared to an iron-dominated quad. The overall
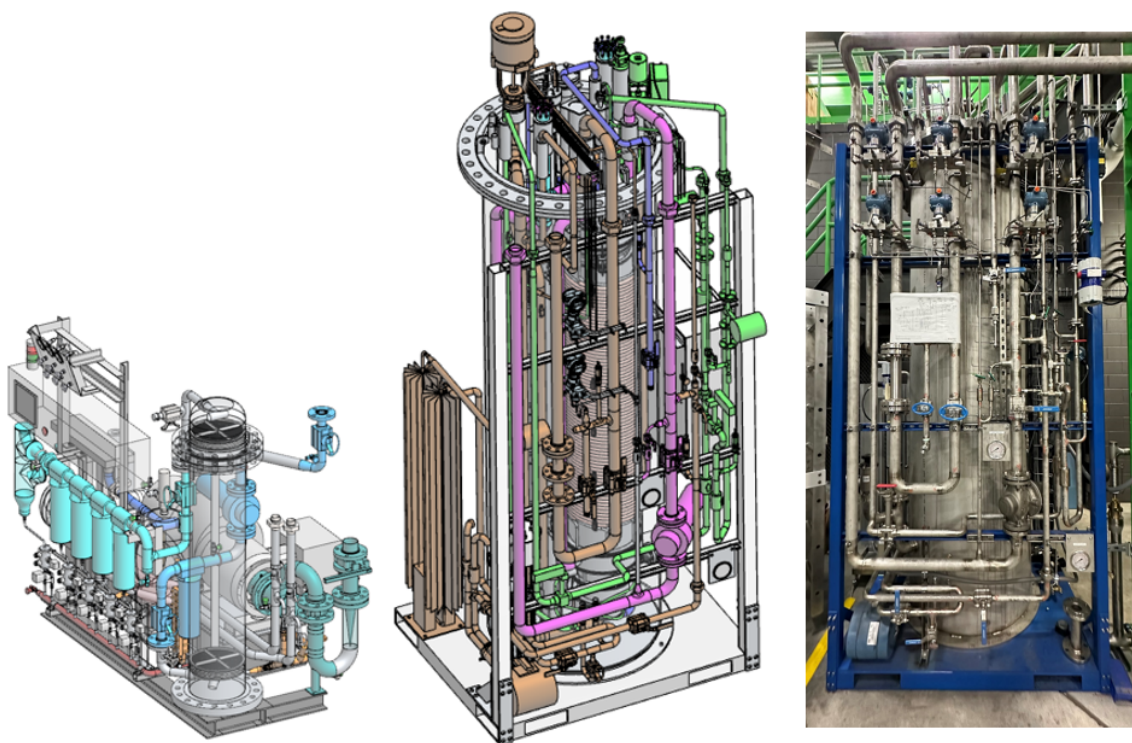
Figure 16. Left: helium recovery compressor design. Middle: cold box design for helium purifier. Right: as-built purifier skid.

approach includes an initial study using a single-layer sub-scale quadrupole to validate both fabrication feasibility and magnetic field performance. Work on the full-scale quadrupole was started in parallel with the small-scale effort. As shown in figure 17, manufacturing and testing proceeds along a sequential path, including bobbin design and fabrication, winding, over-banding, splicing, impregnation, coil assembly, and cold testing. Substantial engineering efforts have been dedicated to refining precision bobbin machining techniques to establish the desired quadrupole current path for high field quality. The sub-scale coil has been successfully wound, and we anticipate cold-testing it in the fall of 2024.

6.3 Controls

The FRIB project scope was limited to the exit of the fragment separator that supplies the secondary beam lines originally part of NSCL. The control system for the secondary beam lines must be upgraded to meet the standards of the FRIB control system to improve network security and maintainability. A 3-phase upgrade is planned: (1) transitioning the control system from the NSCL network to the new secure FRIB control network; (2) replacing obsolete control devices to mitigate network security risks and improve maintainability; (3) replacing control devices with standardized FRIB devices for efficient maintenance and reduced spare inventory. Phases 1 and 2 are mostly complete, while Phase 3 is ongoing.
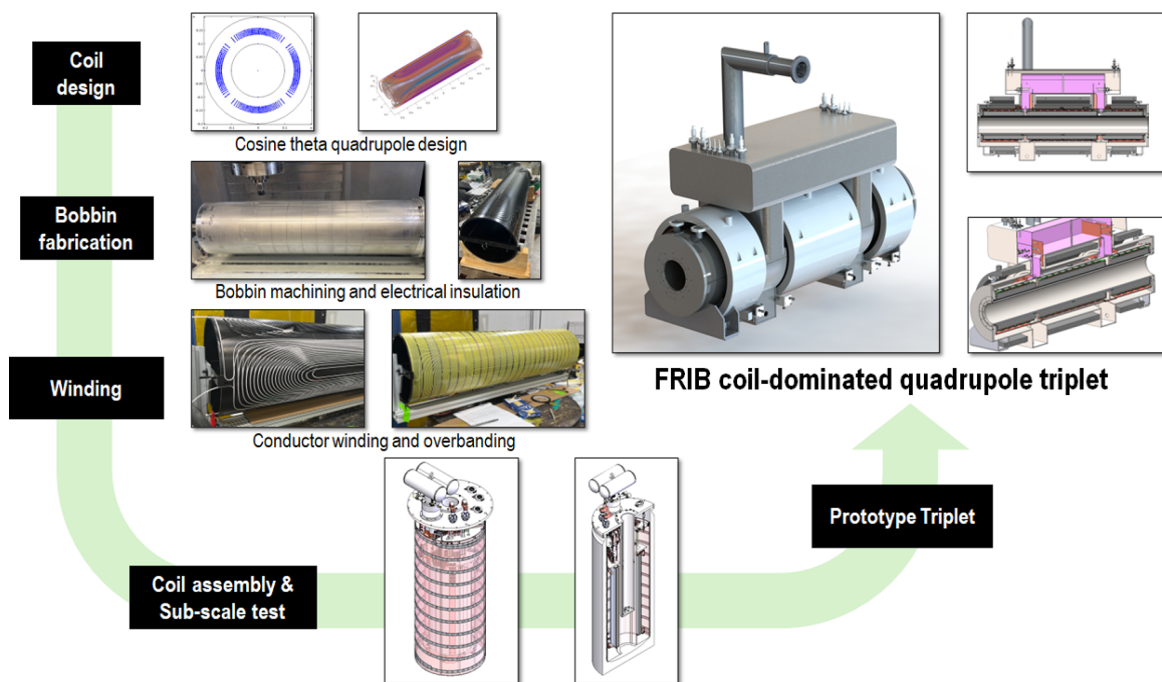
Figure 17. Development steps for the FRIB Coil-Dominated Quadrupole (CDQ).

7 Automation and machine learning

Automation is important both for high-availability operation and the power ramp-up. For a facility consisting of hundreds of beam line devices, efficient operation is only possible through automation. Moreover, automation can reduce human error, reduce training efforts, and improve operational consistency; for tasks that require a faster reaction time than humanly possible, for example quick recovery from a trip, automation is the only solution [36].

FRIB linac automation is being implemented at both the device level and the system level. At the device level, turn-on/turn-off for a cavity or solenoid is programmed in the input-output controller (IOC) using state notation language (SNL). At the system level, a few buttons on the graphical user interface (GUI) may be used for sending auto-on/off commands to devices throughout the linac, executed at the device level. This is usually implemented with Python scripts, which provide great flexibility. Python scripts are also used for prototyping device-level tasks at the early stages when frequent and quick iterations are necessary.

Machine learning (ML) may facilitate challenging tasks for efficient high-power operation, especially tasks that involve a large number of variables and cases in which the interaction between variables is complex or difficult to characterize analytically.

7.1 Automation of room temperature devices

Automatic turn-on and fast recovery algorithms have been implemented for all room temperature devices. When turning on a high-power room-temperature RF cavity, such as the RFQ or FS1 buncher [37], a slow power ramp-up is preferable to avoid excessive thermal gradients. During the power ramp-up, the pressure in the beam line vacuum system may increase due to the temperature rise

or electric discharges. Depending on the cavity history and ramp rate, there may be some risk that the pressure will exceed the trip level. To reduce this risk, the power ramp-up rate is automatically adjusted while monitoring the pressure read-back, as shown in figure 18(a). The cavities are turned on in self-excited loop (SEL) mode such that the RF drive frequency tracks the cavity resonant frequency. When the transient detuning subsides, the operating mode automatically switches to the generator driven resonator (GDR) mode.

Figure 18(b) shows an example of automation for fast recovery after an RFQ trip. If a trip is detected and found to be recoverable, the operating mode immediately switches to SEL, and the field is restored within 3 to 5 seconds, which allows us to avoid excessive detuning from thermal transients. The algorithm switches back to GDR mode if the detuning is small enough to resume beam operation. Without automatic recovery, it may take 20 to 30 minutes to resume beam operation instead of 10 to 20 seconds due to the slow response of the temperature-based RFQ frequency control loop. Development efforts using ML have been initiated to further optimize frequency control of the RFQ and further reduce the downtime due to transients [38], as discussed in section 7.3.
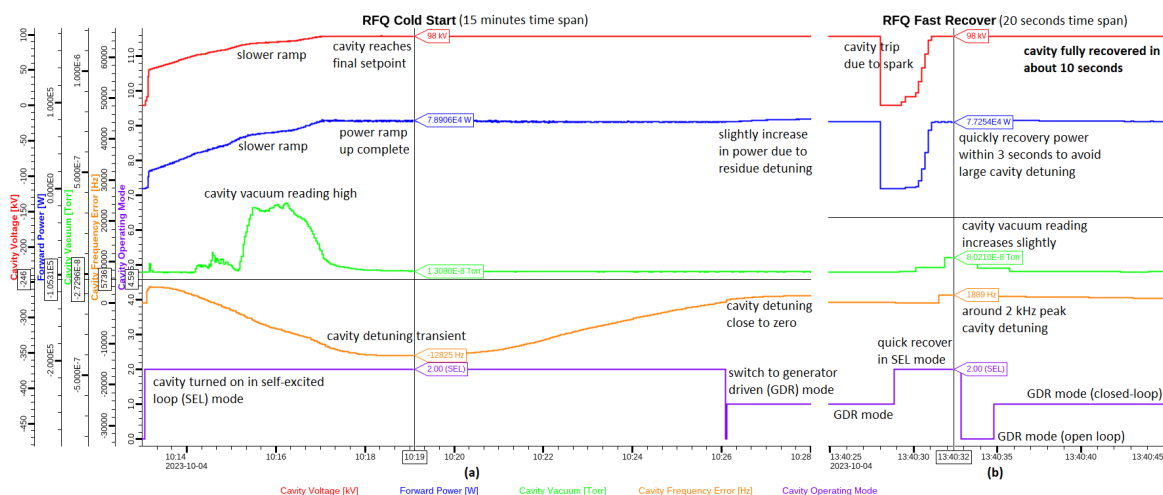
Figure 18. Examples of automation for the FRIB room-temperature RFQ: (a) auto turn-on from cold condition; (b) fast recovery from a trip.

7.2 Cryomodule automation

Though there are a few room-temperature devices, the FRIB linac is mainly composed of SRF cryomodules (a total of 46 cryomodules operating at 4.5 K or 2 K). Automation helps to reduce the time needed for turn-on, tuning, and turn-off of the SRF cavities and SC magnets [39] and hence allows more time for beam operation, which eventually facilitates beam power ramp-up.

One example is automatic turn-on of all SRF cavities, which is now a major asset for linac operation for the FRIB FSEE user program [40]. The FSEE users require frequent access the FSEE experimental area downstream of Linac Segment 1 to switch samples, sometimes more than once per hour. All SRF cavities must be turned off for each access. Automation with control of the cryomodule internal heaters allows us to turn off all cavities in less than 1 minute and turn them back on in about 2 minutes, as shown in figure 19. The heaters compensate for the change in the load to the cryogenic plant, maintaining stable temperatures and bath pressures.
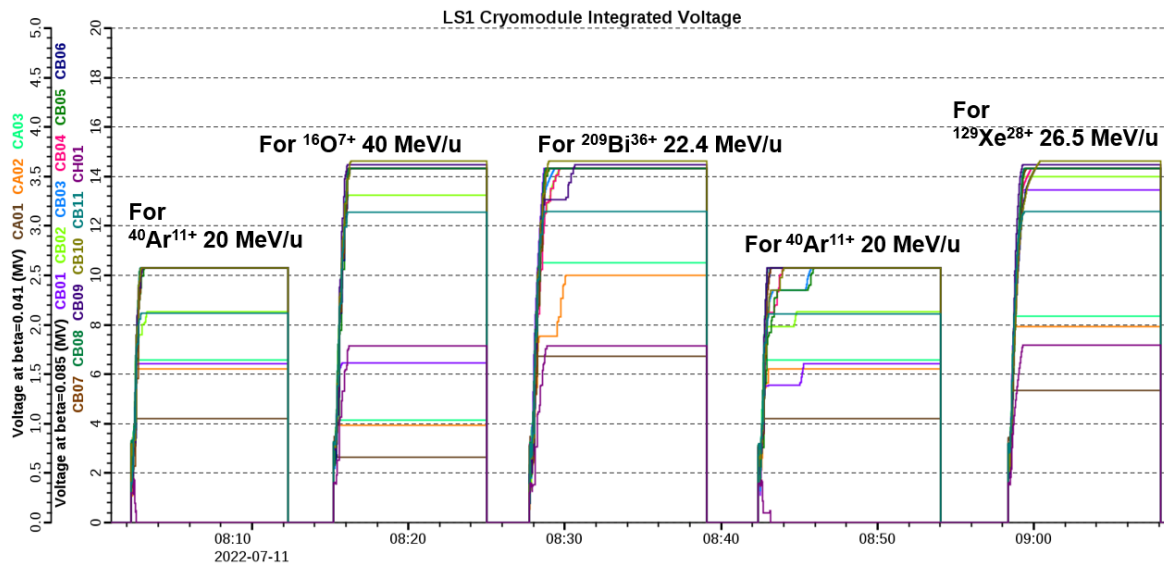
Figure 19. Example of fast turn-on/turn-off of LS1 (104 SRF cavities) with transitions to different ion beams during FSEE operations.

Other tasks related to linac operation that have been automated include field "reduce and recover" for cavities with high field emission; pneumatic tuner valve calibration for half wave resonators (HWRs); conditioning of cavity multipacting; magnet degaussing; and linac emergency shutdown [39].

7.3 Artificial intelligence and machine learning

ML may become an essential tool for boosting FRIB beam power and ensuring efficient and safe operation. Leveraging real-time and archived operational data, ML techniques could create data-driven models, which may be useful for faster beam tuning, improved control of beam losses, fast anomaly detection, and designing advanced controls for accelerator hardware.

ML has been used for accelerators to construct surrogate models that encapsulate the highly non-linear and high-dimensional dynamics of beams and accelerator components. Data-driven techniques are particularly valuable when conventional physics-based models are either absent or excessively intensive in computation time. In the FRIB front end, an ML-based surrogate model has been built for the Bayesian optimization of the transmission through the RFQ. The ML-based optimization searches the parameter space globally and converges to a solution with higher transmission than past results with traditional local optimization methods [41]. In addition to beam centering, ML may be used to reconstruct the beam phase space distribution from measured projections on profile monitors (tomography). An ML-based tomography method for reconstructing the 4-D beam distribution has been studied [42].

ML techniques can be applied not only to beam tuning and optimization, but also to control of accelerator devices. For example, an ML-based dynamic model was developed recently for control of the RFQ temperature, which is used for frequency tuning. The model predicts the temperature and frequency based on the water flow and the RF forward power. To account for the response time of the system, a Long Short-Term Memory (LSTM) model is used, along with a Koopman Operator technique which linearizes the (highly nonlinear) dynamic system. The ML-based model takes 300

seconds of historical data, including the RF frequency, water flow rate, and water temperature, to predict the frequency of the RFQ for the next 300 seconds. As shown in figure 20, the model predicts the frequency reliably in most cases, except for rare cases such as a sudden frequency jump due to an abrupt forward power change (figure 20(k)). By combining the control model of the RFQ and an optimization method such as the Newton-Raphson method, simulations show that this ML-based predictive control method has the potential to reduce the RFQ tuning time by factor of 2 compared with a traditional Proportional-Integral-Derivative (PID) control method [38].
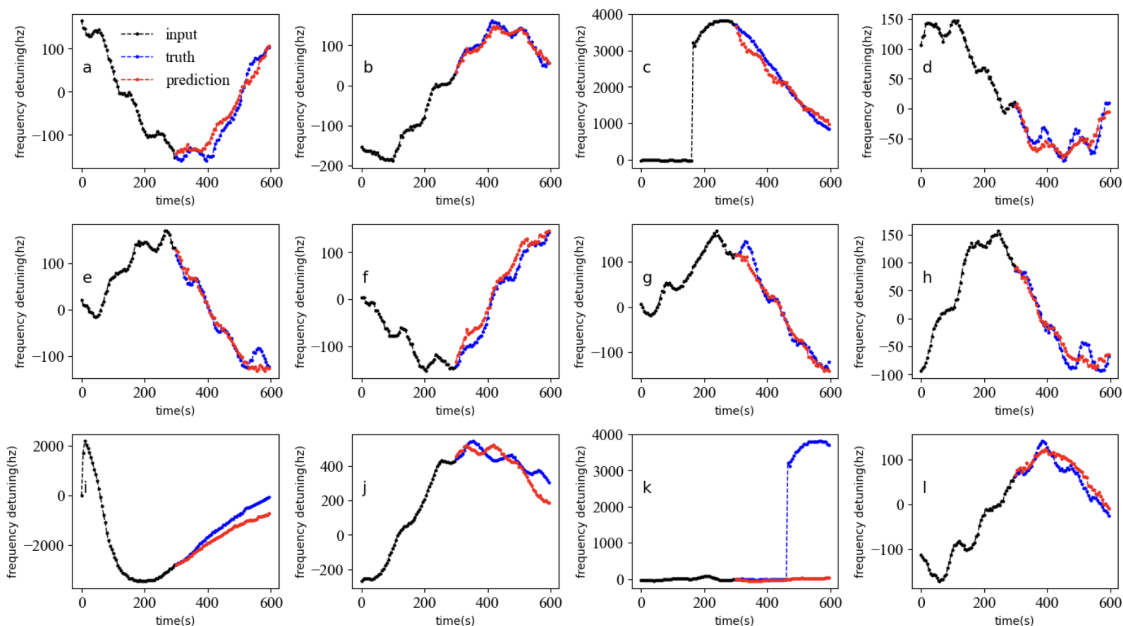
Figure 20. Examples of frequency prediction for the RFQ using an AI/ML model for 12 different cases. The black dots (0 to 300 s) represent historical frequency detuning data (the difference between the resonant frequency and the frequency set point). The blue and red dots (300 to 600 s) represent the measured and predicted frequency detuning, respectively.

8 Conclusion

FRIB has been operating for more than a year, delivering beams for both scientific and industrial experiments with the desired reliability and availability. The primary beam power has been steadily raised from 1 to 10 kW. To ramp up to the ultimate design beam power of 400 kW, efforts are focused on phased linac and ARIS improvements, phased targetry system deployments, control of beam loss and radiological impacts, legacy system renovation, automation, and machine learning. The power ramp-up campaign and the proposed FRIB upgrade to double the primary-beam energy to 400 MeV/nucleon [43] will significantly enhance FRIB's discovery potential.

Acknowledgments

FRIB accelerator systems design and construction have been facilitated under work-for-others agreements with many DOE-SC national laboratories including ANL, BNL, FNAL, JLab, LANL,

References

[1] J. Wei et al., *Accelerator commissioning and rare isotope identification at the Facility for Rare Isotope Beams*, *Mod. Phys. Lett. A* **37** (2022) 2230006.

[2] P.N. Ostroumov et al., *First Simultaneous Acceleration of Multiple Charge States of Heavy Ion Beams in a Large-Scale Superconducting Linear Accelerator*, *Phys. Rev. Lett.* **126** (2021) 114801.

[3] T. Kanemura et al., *Experimental Demonstration of the Thin-Film Liquid-Metal Jet as a Charge Stripper*, *Phys. Rev. Lett.* **128** (2022) 212301.

[4] H. Ren et al., *Development and status of the FRIB 28 GHz SC ECRIS*, *J. Phys. Conf. Ser.* **2244** (2022) 012008.

[5] F. Pellemoine et al., *Thermo-mechanical behaviour of a single slice test device for the FRIB high power target*, *Nucl. Instrum. Meth. A* **655** (2011) 3.

[6] T. Xu et al., *Completion of FRIB Superconducting Linac and Phased Beam Commissioning*, *JACoW* **SRF2021** (2022) MOOFAV10.

[7] J. Wei et al., *FRIB Transition to User Operations, Power Ramp Up, and Upgrade Perspectives*, *JACoW* **SRF2023** (2023) MOIAA01.

[8] W. Hartung et al., *Investigation of Plasma Processing for Coaxial Resonators*, *JACoW* **SRF2023** (2023) THIXA01.

[9] J. Guo et al., *FRIB ECR ion sources operation and future development*, presented at the *International Conference on Ion Sources*, Victoria, BC, Canada, Sep. 2023, Talk 131.

[10] T. Shen et al., *Design and Development of a 28 GHz Nb$_3$Sn ECR Ion Source Superconducting Magnet*, *IEEE Trans. Appl. Superconduct.* **34** (2024) 4301105.

[11] L.T. Sun et al., *Low energy beam transport for facility for rare isotope beams driver linear particle accelerator*, *Rev. Sci. Instrum.* **83** (2012) 02B705.

[12] P.N. Ostroumov, K.W. Shepard, V.N. Aseev and A.A. Kolomiets, *Heavy ion beam acceleration of two charge states from an ECR ion source*, in the proceedings of the *20th International Linear Accelerator Conference*, Monterey, CA, U.S.A., 21–25 August 2000, pp. 202–204 [`physics/0008184`].

[13] P. Ostroumov et al., *Accelerator Physics Advances in FRIB (Facility for Rare Isotope Beams)*, in the proceedings of the *9th International Particle Accelerator Conference*, Vancouver, Canada, 29 April–4 May 2018, pp. 2950–2952 [`DOI:10.18429/JACoW-IPAC2018-THYGBF4`].

[14] S. Lidia et al., *Overview of Beam Diagnostic Systems for FRIB*, in the proceedings of the *4th International Beam Instrumentation Conference*, Melbourne, Australia, 13–17 September 2015, pp. 226–230 [`DOI:10.18429/JACoW-IBIC2015-MOPB071`].

[15] S. Cogan, S. Lidia and R. Webber, *Diagnostic Data Acquisition Strategies at FRIB*, in the proceedings of the *5th International Beam Instrumentation Conference*, Barcelona, Spain, 11–15 September 2016 [`DOI:10.18429/JACoW-IBIC2016-WEAL03`].

[16] S. Lidia, *Beam Diagnostics for FRIB Commissioning*, presenteed at the *11th International Beam Instrumentation Conference*, Kraków, Poland, 11–15 September 2022, Talk MO2I1, https://accelconf.web.cern.ch/ibic2022/talks/mo2i1_talk.pdf.

[17] A. Lokey and S. Lidia, *Status of Gas Sheet Monitor for Profile Measurements at FRIB*, *JACoW* **IBIC2023** (2023) WEP027.

[18] M. Yoshimoto et al., *Development of the Beam Loss Monitor for Beam Halo Measurement in the J-PARC RCS*, in the proceedings of the *4th International Beam Instrumentation Conference*, Melbourne, Australia, 13–17 September 2015, pp. 575–579 [`DOI:10.18429/JACoW-IBIC2015-WEBLA02`].

[19] M. Avilov et al., *Thermal, mechanical and fluid flow aspects of the high power beam dump for FRIB*, *Nucl. Instrum. Meth. B* **376** (2016) 24.

[20] M. Hausmann et al., *Design of the Advanced Rare Isotope Separator ARIS at FRIB*, *Nucl. Instrum. Meth. B* **317** (2013) 349.

[21] M. Portillo et al., *Commissioning of the Advanced Rare Isotope Separator ARIS at FRIB*, *Nucl. Instrum. Meth. B* **540** (2023) 151.

[22] D. Swan, J. Yurkon and D.J. Morrissey, *A simple two-dimensional PPAC*, *Nucl. Instrum. Meth. A* **348** (1994) 314.

[23] M. Cortesi, J. Yurkon and A. Stolz, *Measurements of secondary scintillation in low-pressure CF(4) with a SiPM, from a parallel-plate avalanche geometry*, 2016 *JINST* **11** P04017.

[24] M. Cortesi, Y. Ayyada and J. Yurkon, *Development of a Parallel-Plate Avalanche Counter with Optical Readout (O-PPAC)*, 2018 *JINST* **13** P10006 [`arXiv:1808.05882`].

[25] O.B. Tarasov and D. Bazin, *LISE++: Radioactive beam production with in-flight separators*, *Nucl. Instrum. Meth. B* **266** (2008) 4657.

[26] O.B. Tarasov et al., *LISE$_{cute}^{++}$, the latest generation of the LISE^{++} package, to simulate rare isotope production with fragment-separators*, *Nucl. Instrum. Meth. B* **541** (2023) 4.

[27] P. Knudsen et al., *FRIB helium refrigeration system commissioning and performance test results*, *IOP Conf. Ser. Mater. Sci. Eng.* **755** (2020) 012090.

[28] N. Hasan et al., *Design, Fabrication and Installation of the Cryogenic Distribution System for Re-Configured FRIB A1900 Fragment Separator*, in *International Cryogenic Engineering Conference and International Cryogenic Materials Conference*, L. Qiu, K. Wang and Y. Ma, eds., Springer Nature Singapore (2023), p. 233–239 [`DOI:10.1007/978-981-99-6128-3_28`].

[29] N. Hasan, V. Ganni and P. Knudsen, *Analysis and Management of Thermal Energy Release During Quench in a Superconducting Magnet*, in the proceedings of the *ASME International Mechanical Engineering Congress and Exposition*, Columbus, OH, U.S.A., 30 October–3 November 2022, vol. 8, V008T10A012 [`DOI:10.1115/imece2022-95762`].

[30] N. Hasan et al., *Design, fabrication, and installation of the cryogenic distribution system for FRIB target and fragment pre-separator superconducting magnets*, *IOP Conf. Ser. Mater. Sci. Eng.* **1240** (2022) 012083.

[31] N. Hasan et al., *Commissioning and Operational Experience from FRIB Target and Fragment Pre-separator Superconducting Magnet Quench Management System*, in *Advanced Topics in Science and Technology in China*, L. Qiu, K. Wang and Y. Ma, eds., Springer Nature Singapore (2023), p. 249–255 [`DOI:10.1007/978-981-99-6128-3_30`].

[32] V. Ganni, P. Knudsen and J.G. Weisend, *Optimal Design and Operation of Helium Refrigeration Systems Using the Ganni Cycle*, *AIP Conf. Proc.* **1218** (2010) 1057.

[33] Y. Choi et al., *Overview of Fragment Separator Superconducting Magnets in the Facility for Rare Isotope Beams*, *IEEE Trans. Appl. Superconduct.* **33** (2023) 1.

[34] D. Greene et al., *Design of Coil-Dominated Quadrupole Triplet for High Rigidity Isotope Beams*, *IEEE Trans. Appl. Superconduct.* **33** (2023) 1.

[35] P.L. Walstrom, *Design of end turns in current-dominated dipole and quadrupole magnets for fields with low higher-harmonic content*, in the proceedings of the *8th European Particle Accelerator Conference*, Paris, France, 3–7 June 2002, pp. 2448–2450, https://accelconf.web.cern.ch/e02/PAPERS/MOPLE008.pdf.

[36] S. Zhao et al., *Automation of RF and Cryomodule Operation at FRIB*, *JACoW* **HIAT2022** (2022) TH1C3.

[37] P.N. Ostroumov et al., *Efficient continuous wave accelerating structure for ion beams*, *Phys. Rev. Accel. Beams* **23** (2020) 042002.

[38] J. Wan, S. Zhao, W. Chang and Y. Hao, *Time-Delayed Koopman Network-Based Model Predictive Control for the FRIB RFQ*, `arXiv:2401.11031`.

[39] W. Chang et al., *Automation of FRIB SRF Cavities and SC Solenoids Turn-on/off*, *JACoW* **SRF2023** (2023) FRIBA05.

[40] S. Lidia et al., *A Heavy-Ion Single-Event Effects Test Facility at Michigan State University*, in the proceedings of the *2IEEE Radiation Effects Data Workshop (REDW) (in conjunction with 2022 NSREC)*, Provo, UT, U.S.A., 18–22 July 2022 [`DOI:10.1109/redw56037.2022.9921718`].

[41] P. Ostroumov et al., *FRIB from Commissioning to Operation*, in the proceedings of the 68th *ICFA Advanced Beam Dynamics Workshop on High-Intensity and High-Brightness Hadron Beams — HB2023*, Geneva, Switzerland, 9–13 October 2023, pp. 9–15 [`DOI:10.18429/JACoW-HB2023-MOA1I2`]

[42] A. Tran and Y. Hao, *Beam tomography with coupling using maximum entropy technique*, *JACoW* **IPAC2023** (2023) THOGB2.

[43] FRIB Science Community, *FRIB400: The Scientific Case for the 400 MeV/u Energy Upgrade of FRIB*, Tech. Rep., FRIB, Michigan State University, East Lansing, MI, U.S.A. (2019), https://frib.msu.edu/sites/default/files/_files/pdfs/frib400_final.pdf.

[44] J. Wei et al., *FRIB Beam Power Ramp-up: Status and Plans*, in the proceedings of the 68th *ICFA Advanced Beam Dynamics Workshop on High-Intensity and High-Brightness Hadron Beams — HB2023*, Geneva, Switzerland, 9–13 October 2023, pp. 351–357 [`DOI:10.18429/JACoW-HB2023-THC1I2`]